Journal of Alloys and Compounds 509 (2011) 8999–9004

Contents lists available at ScienceDirect

Journal of Alloys and Compounds

journal homepage: www.elsevier.com/locate/jallcom

Structural, magnetic and Mössbauer spectral studies of nanocrystalline $Ni_{0.5}Zn_{0.5}Fe_2O_4$ ferrite powders

Seema Verma [a,*], P.A. Joy [b], Sajith Kurian [c]

[a] Department of Chemistry, Indian Institute of Science Education and Research (IISER), 900, NCL Innovation Park, Dr Homi Bhabha Road, Pune 411 008, India
[b] Physical and Materials Chemistry Division, National Chemical Laboratory, Pune 411 008, India
[c] Department of Chemistry, Indian Institute of Technology, Kanpur 208 016, India

ARTICLE INFO

Article history:
Received 1 December 2010
Received in revised form 9 June 2011
Accepted 13 June 2011
Available online 6 July 2011

Keywords:
Nanostructured materials
Chemical synthesis
Magnetisation
Mössbauer spectroscopy

ABSTRACT

Nanocrystalline $Ni_{0.5}Zn_{0.5}Fe_2O_4$ powders, synthesized by a combustion method are investigated by X-ray diffraction, vibrating sample magnetometry and Mössbauer spectroscopic techniques. We adopt a strategy to systematically control the particle sizes between 4 and 45 nm simply by changing the elemental stoichiometric coefficient, Φ_e, of the combustion mixture. Curie temperature of the superparamagnetic particles of size 4 nm is higher than that of the bulk particles. Interestingly, bigger particles (45 nm) show a comparable room temperature saturation magnetization and exceptionally very high Curie temperature of 833 K, when compared to that of the bulk $Ni_{0.5}Zn_{0.5}Fe_2O_4$ material (563 K).

1. Introduction

NiZn ferrite with the spinel structure is a soft magnetic material exhibiting high electrical resistivity and high magnetic permeability, especially suitable for many applications at high frequencies, e.g. antenna rods, suppression of electromagnetic interference, broad band transformers, etc. [1,2]. Magnetic properties of the ferrites are mainly governed by the types of ions and their distribution in two crystallographic sites [1,3]. For NiZn ferrite, $Ni_{1-x}Zn_xFe_2O_4$, the cation Zn^{2+}, Fe^{3+} and Ni^{2+} are distributed in the tetrahedral (A) and octahedral (B) sites of a face centered cubic lattice formed by O^{2-} ions. It is well established that Zn^{2+} and Ni^{2+} ions have a strong preference for the tetrahedral and octahedral sites, respectively and pure phase of NiZn ferrite is thus expected to have a cation distribution represented by $(Zn_xFe_{\{1-x\}})_A[Ni_{\{1-x\}}Fe_{\{1+x\}}]_BO_4$. Fe^{3+} on the other hand has a strong preference for the tetrahedral sites as compared to the octahedral sites. Therefore, comparatively, the formation of $NiFe_2O_4$-type structure is most favorable as both $Fe^{3+}$and Ni^{2+} occupy their preferred sites with ease. However, with the introduction of Zn^{2+} in the system, a less favorable situation of Zn^{2+} pushing Fe^{3+} to the octahedral site arises.

Over the past few years there has been an increased interest in the study of nanocrystalline magnetic materials due to their broad range of application potentialities such as in high density magnetic storage, magnetic carriers for site specific drug delivery and contrast enhancement in magnetic resonance imaging [4–6]. Importantly, nanosized ferrite particles exhibit unusual magnetic properties, which are not observed in the bulk, such as single domain behavior, superparamagnetism, metastable cation distribution, reduced magnetization due to surface spin canting, spin glass behavior and enhancement in the Curie temperature [7–11]. Surface spin canting and collective magnetic excitation in superparamagnetic particles lower its magnetization which severely limit the applications of nanosized ferrite particles. Therefore understanding and controlling the superparamagnetic features of nanoparticles is important in order to fine tune the magnetic properties for many potential applications including ferrofluid technology and magnetic hyperthermia [12,13]. Several attempts have also been made in the direction to synthesize nanosized $Ni_{1-x}Zn_x$ ferrites, so as to obtain good dielectric properties and high performance at relatively lower sintering temperature [14,15]. The formation of pure phase of nanosized NiZn ferrite depends sensitively upon synthetic routes. Among all the wet chemical synthetic routes, glycine nitrate process (GNP) of combustion synthesis is an important processing technique [16]. GNP is rapid, self-sustaining and occurs at a low decomposition temperature of 200 °C. For the complete combustion reaction to take place a stoichiometric molar ratio of the oxidizer such as metal nitrates and a fuel such as glycine is required, as shown in the following equation:

$$0.5Ni(NO_3)_2 \cdot 6H_2O + 0.5Zn(NO_3)_2 \cdot 6H_2O + 2\,Fe(NO_3)_3 \cdot 9H_2O + \frac{40}{9}NH_2CH_2COOH \rightarrow Ni_{0.5}Zn_{0.5}Fe_2O_4 + \frac{80}{9}CO_2 + \frac{100}{9}H_2O + \frac{56}{9}N_2$$

* Corresponding author. Tel.: +91 20 2590 8072; fax: +91 20 2589 9790.
E-mail address: sa.verma@iiserpune.ac.in (S. Verma).

0925-8388/$ – see front matter © 2011 Elsevier B.V. All rights reserved.
doi:10.1016/j.jallcom.2011.06.047

Table 1
Sample code, metals to glycine molar ratio used for the synthesis and XRD data of NiZn ferrite obtained at 473 K.

Sample code	Metal to glycine molar ratio	XRD particle size (±1) nm	Lattice parameter (Å)
G1	1:0.25	4	8.402(2)
G2	1:0.5	8	8.392(4)
G3	1:1.0	24	8.388(1)
G4	1:1.5	45	8.380(5)
G5[a]	1:2.0	55	8.379(2)

[a] Impurities as ZnO, NiO and other phases detected.

The stoichiometry of the combustion mixture is expressed in terms of the elemental stoichiometric coefficient, Φ_e, a parameter used to describe the ratio of the fuel to oxidizer in a combustion mixtures [17,18]. This is defined as,

$$\Phi_e = \frac{\sum(\text{coefficient of oxidizing elements in specific formula}) \times (\text{valency})}{(-1)\sum(\text{coefficient of reducing elements in specific formula}) \times (\text{valency})}$$

It is known that the chemical energy released from the exothermic reaction can be varied with the change in Φ_e, thereby changing the local heat of the system associated with the corresponding combustion reactions. The mixture is stoichiometric when $\Phi_e = 1$, fuel-lean when $\Phi_e > 1$ and fuel-rich when $\Phi_e < 1$. This can allow a systematic variation of the particle size obtained by controlling the metal nitrate to glycine molar ratio [19]. With stoichiometric and fuel rich combustion mixtures, the GNP method is well known to give rise to inhomogeneous phases with submicron size particles. However, with fuel lean combustion mixture, an appropriate metal nitrate to glycine molar ratio with an optimum complexant and controlled combustion nature of glycine may offer a suitable flame temperature near-smoldering combustion behavior to obtain stable spinel nanoparticles [20]. In the present investigation we adopt a strategy of varying elemental stoichiometric coefficient, Φ_e to systematically change the sizes and structures of the spinel formed. It is therefore expected that the magnetic characteristics of the NiZn, $Ni_{0.5}Zn_{0.5}Fe_2O_4$ ferrite particles synthesized by GNP will be strongly dependent upon the combustion reactions with varying Φ_e. It is also expected that multipoint rapid decomposition of the complex with the simultaneous evolution of large amount of gases favors the formation of nearly monodispersed nanoparticles [19,20]. We demonstrate this aspect in the present investigation.

Studies on various aspects of nanocrystalline ferrites, synthesized by different wet chemical methods, have been reported in the literature [9,21–28]. For $MnFe_2O_4$, an increase in the Curie temperature as high as 97 K, when compared with that of the bulk material is reported, when the particle size is reduced to 7.5 nm [9]. Though these changes have been explained in terms of finite size scaling, it was later explained in terms of the changes in the distribution of cations in the two different sites of the ferrite lattice, because from finite size scaling effects a decrease in the Curie temperature from that of the bulk is expected [29–32]. Such enhancement in Curie temperature is also observed for nanosized $NiFe_2O_4$ and $Ni_{0.5}Zn_{0.5}Fe_2O_4$ [26,27].

In the present investigation we adopt the strategy of varying elemental stoichiometric coefficient, Φ_e to systematically control the sizes and structures of the spinel formed. We report the observation of unusual magnetic behavior in the case of nanocrystalline $Ni_{0.5}Zn_{0.5}Fe_2O_4$ powders of varying sizes. It is found that the Curie temperature of the ferrite with size 4 (±1) nm is above that of the bulk materials and it further increases with increasing particle sizes. Increase in the Curie temperature, as high as 270 K is observed for NiZn ferrite of 45 (±1) nm size obtained from this method. This unusual increase in the Curie temperature is explained on the basis of an interesting evolution of off-stoichiometric mixed spinel phase representing different cation distributions in the spinel lattice.

2. Experimental

$Ni_{0.5}Zn_{0.5}Fe_2O_4$ was synthesized from AR grade chemicals by the following steps. Zinc nitrate was prepared by dissolving zinc powder in 8 N nitric acid. An appropriate molar ratio of the metal nitrates and glycine were mixed as mentioned in Table 1. The resultant homogeneous solutions thus obtained were boiled under reflux condition for 1 h in a 1 L capacity round bottom flask. Finally the solutions were slowly evaporated on a water bath to form a viscous gel. The gels were allowed to undergo rapid combustion reaction in a preheated furnace at 473 K. The sample was kept at the same temperature for 4 h. The NiZn ferrites of different particle sizes referred to as G1, G2, G3, G4 and G5 as indicated in Table 1 were synthesized. The as-decomposed samples were characterized for its phase purity and crystallinity by powder X-ray diffraction measurements (Philips, PW-1730) with CuKα radiation using Ni filter. Magnetic measurements were carried out using a PAR EG & G 4500 vibrating sample magnetometer (VSM). Field-cooled (FC) and zero-field-cooled (ZFC) magnetization measurements were measured at 50 Oe by the standard procedures. Mössbauer spectroscopy was performed at room temperature using Co^{57} source and the spectra were analyzed using software PCMOS obtained from CMTE-FAST Electronik, Germany.

3. Results and discussion

Fig. 1 shows the powder X-ray diffraction patterns for the NiZn ferrite powders G1, G2, G3, G4, and G5. For G1 (inset Fig. 1), the reflections are extremely broad, indicating nanocrystalline nature of the particles. The decreasing broadening of the different reflections from G2 to G5 indicates increase in the particle size. All the reflections in the XRD patterns correspond to the cubic spinel structure which is corroborated by the simulated pattern for $Ni_{0.5}Zn_{0.5}Fe_2O_4$ (a = 8.382 Å, JCPDS PDF #52-0278). However, for G5 additional reflections due to impurity phases such as NiO and ZnO were observed (~1 5–20%, nominally based upon the XRD relative intensities). It is however interesting to note that though all the reflections in the XRD pattern of G4 corresponds to $Ni_{0.5}Zn_{0.5}Fe_2O_4$ phase, reflections corresponding to (4 0 0) and (4 4 0) planes show asymmetric peaks and therefore presence of weak shoulder corresponding to NiO may not be ruled out [33]. This implies that for G4, formation of NiO may be accompanied by the formation of off-

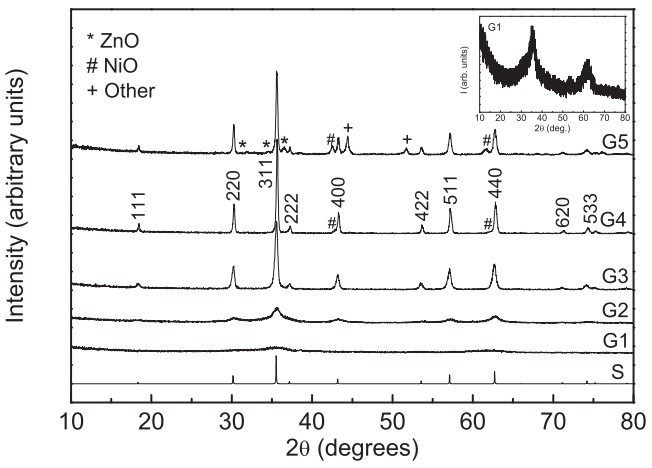

Fig. 1. Powder X-ray diffraction patterns of the different NiZn ferrite powders and (S) simulated XRD pattern $Ni_{0.5}Zn_{0.5}Fe_2O_4$ with a = 8.382 Å.

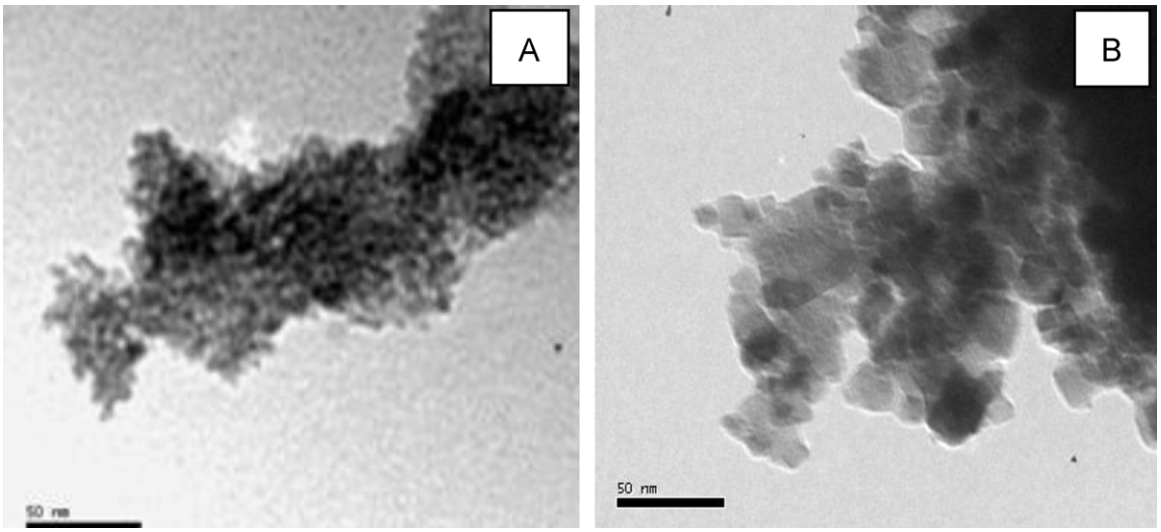

Fig. 2. Transmission electron micrograph of the sample G1 and G4.

stoichiometric NiZn ferrite nanoparticles resulting into the lattice distortion from the ideal spinel structure. However, further structural and magnetic studies are needed to identify and elucidate this possibility.

The average crystallite sizes, as shown in Table 1, were calculated from the XRD line broadening using the Scherrer relationship [34]. The TEM micrographs of G1 and G4, as represented in Fig. 2A and B respectively, show the difference in the particle sizes, as evidenced from the XRD measurements. The cubic lattice parameter values are comparable to that of the bulk values for G4 and G5 and increases slightly with the decrease in the particles size for G1 to G3. The slightly larger lattice parameter for the smaller particles is due to the difference in the cation distributions leading to the increase in the bond stretching and this result compares well with the earlier reports on nanosized $Ni_{0.5}Zn_{0.5}Fe_2O_4$ particles [35,36].

Field dependent magnetization for the NiZn ferrite powders, measured at room temperature, is shown in Fig. 3. The magnetization is very small for G1, which continuously increases with increasing magnetic field and no magnetic hysteresis is observed (see inset A of Fig. 3). This is typical of superparamagnetic behavior as reported for nanoparticles of NiZn ferrite of size less than 10 nm

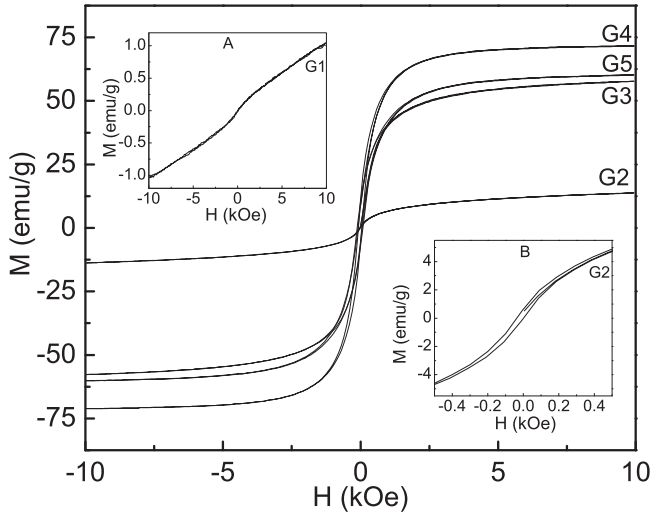

Fig. 3. Field dependent magnetic behavior, measured at 300 K, for G2, G3, G4 and G5. Corresponding magnetization data for G1 is shown in the inset A and enhanced scale magnetization for G2 is shown in the inset B.

[37]. For sample G2, although, no magnetic saturation is observed, a thin hysteresis loop with coercivity of 19 Oe is observed (see inset B of Fig. 3). This indicates for sample G2, there is a wide particle size distribution with larger fraction of small particles and a smaller fraction of large particles (>10 nm) which are not superparamagnetic. For G3 and G4 the coercivity of 103 and 62 Oe respectively is obtained which compares well with the earlier reports where the maximum coercivity is observed for the particles ~30 nm size, which is within the single domain size limit [37,38]. The room temperature saturation magnetization values for the samples G1 and G2 are 1.8 and 16.5 emu/g respectively. The reduced value of the magnetization is likely to be associated with the surface effect arising from the broken exchange interactions and reduced coordination specifically at the surface of each of the particles. Moreover, based upon the shape of the field dependent magnetization of the sample G1, presence of strong canting due to Yafet–Kittel-type spin arrangements may not be ruled out. In the disordered system $Zn_xNi_{1-x}Fe_2O_4$ for $0 \le x \le 1$, presence of the Yafet–Kittel type of canting has been well explained [39]. An increase in the saturation magnetization values of 60 emu/g and 68 emu/g are obtained for the samples G3 and G4 respectively, implying growth of the particles. Interestingly, for the sample G5 with much bigger size of 55 (±1) nm, a decrease in the saturation magnetization value 62.6 emu/g is obtained. Lowering of the magnetic order parameters (MOP) in the sample G5 is expected and this is attributed to the presence of the impurity phases.

The field-cooled (FC) and zero-field-cooled (ZFC) magnetization for the superparamagnetic particles, measured at 50 Oe, is shown in Fig. 4. The maximum in ZFC magnetization for the sample G1, measured at 50 Oe, is at 90 K. The bifurcation of FC and ZFC magnetization above T_B and the continuous increase of magnetization below this temperature indicate existence and distribution of the magnetic anisotropy energy barrier and the slow relaxation of the particles below this temperature. As seen from the inset Fig. 4, much higher and broader T_B of 200 K is obtained for the sample G2, implying the superparamagnetic blocking temperature and the broadness of the maximum increases with increasing particle size and their distribution.

Fig. 5 shows the temperature variation of the magnetization of the samples, measured at a low magnetic field of 50 Oe (Fig. 5A) and at high magnetic field of 5 kOe (Fig. 5B). The Curie temperatures obtained from the low field measurements are 605, 645 and 833 K respectively for the sample G2, G3 and G4. The temperature variation of magnetization of the sample G1 is measured at field

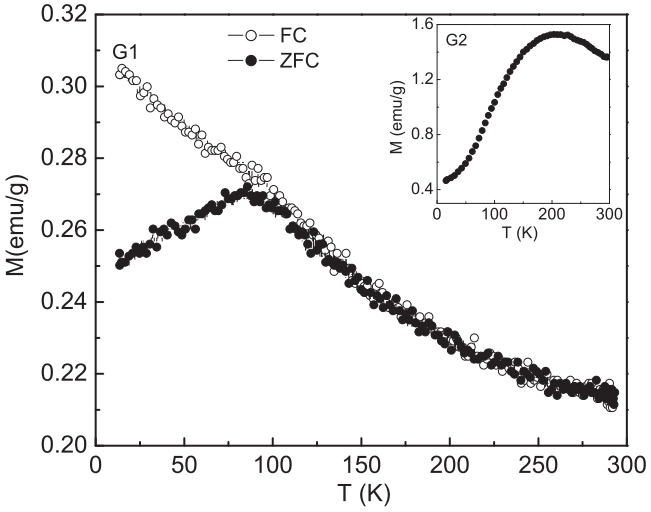

Fig. 4. FC and ZFC magnetization curves of G1, measured at H = 50 Oe, showing the superparamagnetic behavior of G1. Inset: ZFC magnetization curve of G2.

5 kOe (see inset Fig. 5B). The Curie temperature of sample G1 is 573 K. Interestingly, the Curie temperatures of all these samples are larger than the reported value of 563 K for bulk materials [3]. Though, an increase in T_C up to 665 K is reported earlier [27], a change in the Curie temperature to 833 K, as high as 270 K for G4 has never been observed so far. It is known that in the $Ni_{1-x}Zn_xFe_2O_4$ series, the T_C value is highest for $x = 0$, i.e. for $NiFe_2O_4$ (858 K). T_C decreases with increasing Zn content and the highest saturation moment is obtained for the composition with $x = 0.5$ (theoretical 6 μ_B; experimental at 300 K is 3.4 μ_B and at 0 K is 5.2 μ_B), whose T_C is 563 K [3]. The theoretical saturation magnetic moment for

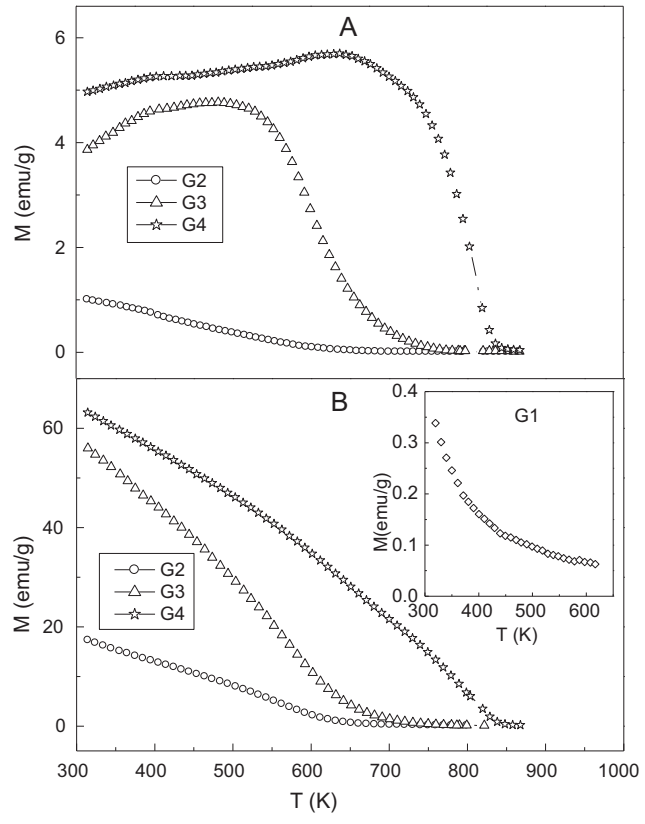

Fig. 5. Temperature variation of the magnetization of samples measured at an applied field of (A) 50 Oe and (B) 5 kOe. Inset B: M vs. T plot for G1 at 5 kOe.

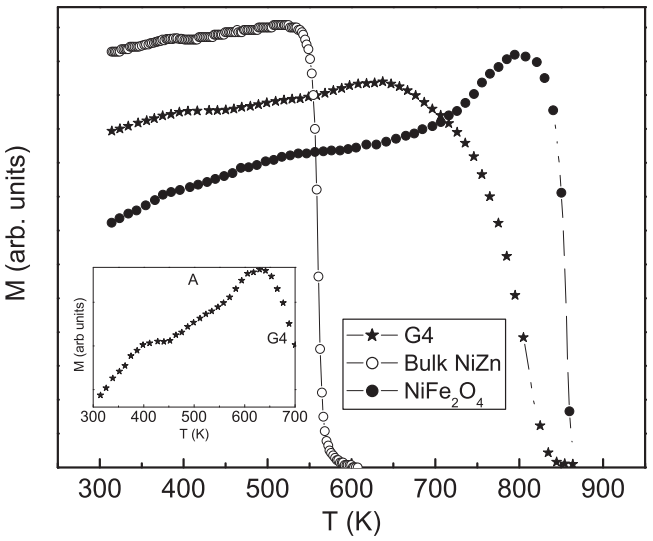

Fig. 6. A comparison of temperature variation of the magnetization of sample G4 with bulk $Ni_{0.5}Zn_{0.5}Fe_2O_4$ and $NiFe_2O_4$ of comparable size, measured at 50 Oe. Inset: Enhanced scale magnetization for G4.

$NiFe_2O_4$ is 2 μ_B whereas the experimental value extrapolated to 0 K is 2.3 μ_B. In the present case, for G4, the T_C is obtained as 833 K, much closer to that of $NiFe_2O_4$. However, the saturation magnetic moment at 300 K is obtained as 2.95 μ_B and the value extrapolated to 0 K is 3.8 μ_B, which are much larger than that of $NiFe_2O_4$. Moreover, the lattice parameter value of 8.380(5) Å is much closer to the value 8.374 Å corresponding to that of bulk NiZn ferrite materials, than that of 8.34 Å for bulk $NiFe_2O_4$ materials. In order to compare the temperature variation of magnetization of the sample G4 with that of the bulk $Ni_{0.5}Zn_{0.5}Fe_2O_4$ material and a pure phase of $NiFe_2O_4$ of comparable size (40 (±1) nm), magnetic measurements on the fresh samples were performed in the small magnetic field of 50 Oe. The $NiFe_2O_4$ sample of comparable size was synthesized by GNP method under identical conditions. The temperature variation of the magnetization of the samples, measured above 300 K, is represented in Fig. 6. For bulk NiZn ferrite, the magnetization curve is similar to that of other multidomain ferrite where the magnetization increases slowly with increase in the temperature and reaches to a broad maximum at a temperature just below the Curie temperature, T_C. On the other hand, the magnetization curve for $NiFe_2O_4$ nanoparticles (40 (±1) nm) the magnetization increases slowly till the temperature ~640 K is reached, above which the magnetization shows a steep rise just below Curie temperature, T_C and further increase in temperature causes demagnetization at the Curie temperature. Interestingly, for the sample G4, the magnetization increases continuously above 300 K with increasing temperature to form a broad maximum at $T_{max1} \sim 400$ K above which the rate of increase of magnetization is slow till the temperature ~560 K and then rapidly increases forming a broad maximum at $T_{max2} \sim 640$ K. This clearly indicates sample G4 is comprised of mixed magnetic phases of different anisotropic energy barriers (see inset A of Fig. 6). Further increase in the temperature results in the demagnetization at T_C of 833 K, which is as high as 270 K, compared to that of the bulk $Ni_{0.5}Zn_{0.5}Fe_2O_4$ material. The cause for this increase in T_C needs to be sought in the presence of mixed magnetic phases on one hand and the formation of off-stoichiometric NiZn phase with different cation distribution favoring enhanced exchange interactions on the other hand.

In order to study the possibility of structural changes, chemical and coordination differences of iron in the nanocrystalline NiZn particles, room temperature ^{57}Fe Mössbauer spectra for the samples are shown in Figs. 7 and 8. Mössbauer spectra of G1 indicate

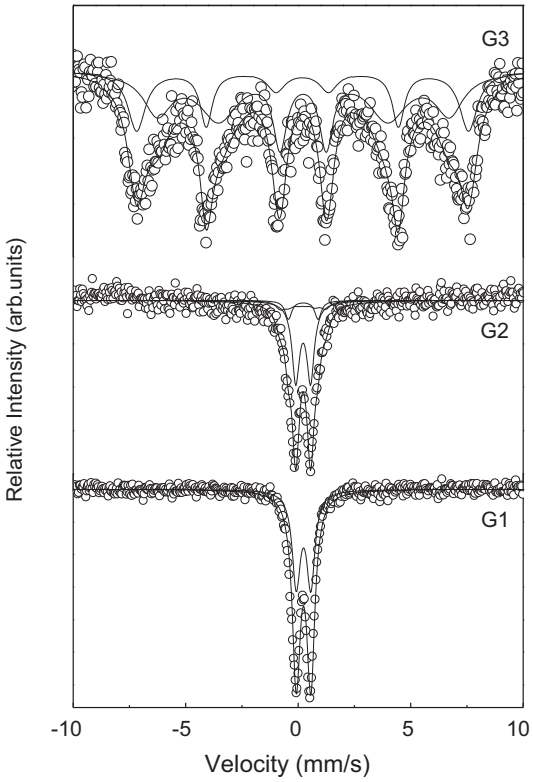

Fig. 7. Room temperature ^{57}Fe Mössbauer spectra of G1, G2 and G3, $Ni_{0.5}Zn_{0.5}Fe_2O_4$ samples.

the superparamagnetic nature of the particles with the isomer shift and line width values of 0.35 mm/s and 0.43 mm/s respectively. Mössbauer spectra of G2 show the presence of one weak magnetic relaxation spectrum and two doublets representing the coexistence of both ferromagnetic and superparamagnetic phases. The isomer shift and line width values of 0.33 (0.05) mm/s and 0.50 (0.01) mm/s respectively are observed for the weak magnetic relaxation spectrum of G2. The observed isomer shift values for the samples G1 and G2 compares well with that of the values reported for Fe^{3+} in NiZn ferrite powders [11,26–28,36,37]. The superparamagnetic doublets in the Mössbauer spectrum account 67% of the relative spectral areas corresponding to Fe^{3+} ions of tetrahedral (A) and octahedral (B) sites. The Mössbauer spectra of G3 are

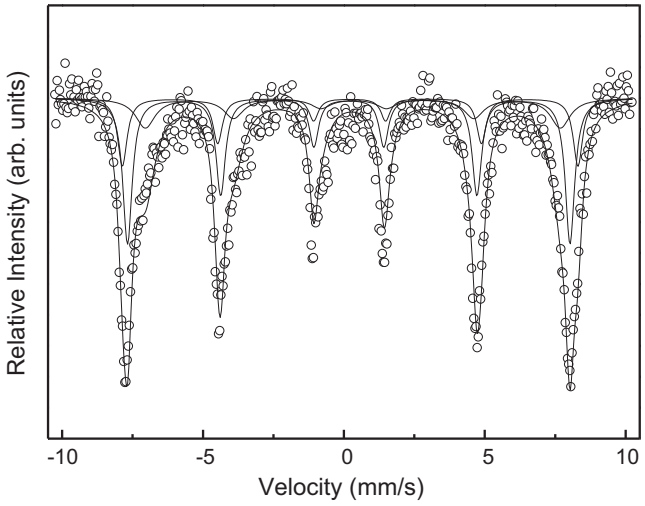

Fig. 8. Room temperature ^{57}Fe Mössbauer spectra of G4, $Ni_{0.5}Zn_{0.5}Fe_2O_4$ sample.

best fitted with two sextets. The unusual spectrum of G3 could be attributed to the reduction in magnetocrystalline anisotropy and large distribution of the magnetic hyperfine fields in the nanoparticles as reported earlier [28,37,40]. The Fe^{3+} ions present in each site are expected to experience a distribution in the magnetic hyperfine field due to the different numbers of nonmagnetic (Zn^{2+}) and magnetic (Ni^{2+}) neighbors and different degrees of collective magnetic excitations for the sample having wide particle size distributions [10,11]. The isomer shift values of δ_{tet} = 0.29 (0.01) mm/s and δ_{oct} = 0.33 (0.02) mm/s are consistent with the high spin Fe^{3+} state. The magnetic hyperfine field (ΔH_{hf}) values of 46 (0.11) T and 41 (0.38) T are observed at the A and B sites respectively, which is smaller than those of the bulk particles [39]. The reduction in the magnetic hyperfine field for the nanoparticles is earlier explained by Morup [41] in terms of collective magnetic excitation. It is important to note that though quasistatic sextet of G3 shows absence of superparamagnetism, decrease in magnetic hyperfine filed could be explained from the collective magnetic excitations. It appears from the recent literature survey in an assembly of single domain NiZn ferrite nanoparticles that even though the particles do not show superparamagnetic behavior in external magnetic field, fluctuations of magnetization along easy axis of magnetization is possible [10,11,27]. In the present study the sample G3 having the size ~24 nm exhibit hysteresis at room temperature whereas slow relaxation of the magnetization vector about easy axis of magnetization has been reported in the Mössbauer spectrum of the sample. This fluctuation of magnetization vector does not collapse the sextets but will act instead to reduce the magnetic hyperfine field and the result is similar to that observed for similar particle sized $Ni_{0.35}Zn_{0.65}Fe_2O_4$ ferrites [11]. The relative area within two sextets for G3 offers interesting observations. For the bulk sample, considering the ideal situation where Zn^{2+} and Ni^{2+} ions prefers to occupy tetrahedral and octahedral sites respectively, the ratio of the intensities of A site to that of B site sextets is 0.33, with the cation distribution of $(Zn^{2+}_{0.5}Fe^{3+}_{0.5})\,[Ni^{2+}_{0.5}Fe^{3+}_{1.5}]\,O_4$. However, it is interesting to observe the ratio of the relative intensities due to the Fe^{3+} at the tetrahedral A site to octahedral B site for G3 is 0.428, which is higher than that of the ideal situation. The expected cation distribution for the sample G3 is therefore $(Zn^{2+}_{0.5}Fe^{3+}_{0.6})\,[Ni^{2+}_{0.5}Fe^{3+}_{1.4}]\,O_4$. This clearly indicates that some of the Fe^{3+} ions from that of B sites is migrated to that of the A site. The enhancement of area corresponding to A sites indicate Fe has occupied more than 8 out of 64 tetrahedral sites in the unit cell, contrary to that of the normal structure of spinel. Similar unusual occupancy of Fe^{3+} in the tetrahedral and octahedral sites has also been reported by others [10,26,27]. It is possible that extremely high chemical energy released from the combustion reaction might have helped to achieve this type of uncommon structure. The enhancement in the A–O–B interactions is mainly achieved by the increase in the number of magnetic Fe^{3+} and/or Ni^{2+} ions in the A sites and this accounts for the enhanced Curie temperature of this sample. Any increase in the A–O–B superexchange bond angle, as indicated by the small increase in the cubic lattice parameter will also contribute to the enhancement of Curie temperature. This type of enhancement in the Curie temperature has been reported in the case of NiZn, $MnFe_2O_4$ and $NiFe_2O_4$ ferrite nanoparticles and has been explained in terms of increase in the strength of superexchange (A–O–B) interactions [26,27,32,42].

Mössbauer spectrum of G4 is shown in Fig. 8. It is interesting to note that the acceptable fit of the spectra was obtained only when the data were fitted with three sextets. Sextet with smallest isomer shift of 0.28 (0.01) mm/s and magnetic hyperfine field of 48.7 (0.2) T is assumed to arise from the Fe^{3+} ions occupying the A sites. Sextet with highest magnetic hyperfine field of 50.13 (0.22) T and isomer shift of 0.32 (0.01) mm/s is assigned to Fe^{3+} ions in the octahedral site. The third sextet with the smallest hyperfine field of 45.7

(0.11) T and isomer shift of 0.44 (0.01) mm/s may be attributed to the second octahedrally coordinated Fe^{3+} ions. For G4, absence of any quadrupole doublet rules out presence of $ZnFe_2O_4$. Therefore, any possibility of segregation of NiZn ferrite to $NiFe_2O_4$ is also ruled out since no impurity phases involving Zn or Ni were detected in the XRD pattern of G4. Formation of Fe_3O_4, for which the lattice parameter is 8.39 Å, saturation magnetization at room temperature is 3.8 μ_B and the Curie temperature is 858 K, can be ruled out due to the absence of Fe^{2+}, as inferred from Mössbauer data. Another possibility for the higher magnetization is the formation of γ-Fe_2O_3, which also can be ruled out as unreacted ZnO were not detected in the powder XRD of G4. Moreover, as the lattice parameter of G4 is comparable to that of the bulk $Ni_{0.5}Zn_{0.5}Fe_2O_4$, it can be concluded that G4 could be the off-stoichiometric NiZn ferrite phase with much improved magnetic properties. The T_C of 839 K corresponds to that of composition with $x = 0.03$ for which the experimental saturation magnetic moment at 0 K is only 2.5 μ_B. Therefore, possibility for the formation of off-stoichiometric mixed spinel phase with much stronger superexchange interaction cannot be ruled out. To analyze complex spectra of G4, we take into considerations that additional Fe^{3+} site apart from the usual tetrahedral and octahedral sites may be attributed to the local structural distortion of ferrite structure due to the formation of off-stoichiometric NiZn sample. The developing NiO type coordination (see XRD reflections corresponding to (4 0 0) and (4 4 0) planes) on the surface of the particles that has not undergone full precipitation may induce frustration in the dipolar system. This may lead to the presence of a much larger proportion of uncompensated surface spins on a ferromagnetic core of off-stoichiometric NiZn lattice. Therefore, the presence of additional Fe^{3+} site can be assigned to the frustrated surface contribution resulting in different environments. There is a direct correlation of the present result with the results obtained earlier on NiZn ferrites studied by Mössbauer spectroscopic technique [28] and spinel type $MgAl_2O_4$ nanoparticles studied by Solid State NMR [43]. However, much further work is clearly needed to elucidate the quantitative description of off-stoichiometric NiZn spinel phase, which is beyond the scope of the present paper. Indeed, in the case of G4, exceptionally high Curie temperature of 833 K is a due to the evolution of off-stoichiometric NiZn ferrite core with frustrated surface spins.

4. Conclusions

Present results show the formation of nanocrystalline $Ni_{0.5}Zn_{0.5}Fe_2O_4$ with unusual magnetic properties when synthesized by a combustion technique utilizing glycine as a fuel. The particle sizes can be systematically controlled simply by changing the elemental stoichiometric coefficient, Φ_e, of the combustion mixture. Curie temperature of the superparamagnetic particles of size 4 (±1) nm is higher than that of the bulk particles. An increase in Curie temperature to 645 K is observed for the intermediate sized particles (24 (±1) nm) and is a result of the deviation of cation occupancy from that of equilibrium distribution in bulk materials. Interestingly, bigger particles (45 (±1) nm) show a comparable room temperature saturation magnetization and exceptionally very high Curie temperature of 833 K, when compared to that of the bulk $Ni_{0.5}Zn_{0.5}Fe_2O_4$ material (563 K). Possibilities of the formation of off-stoichiometric mixed spinel phase with frustrated dipolar system predominantly on the surface of the particles are explored. The relative area belonging to the tetrahedral A and octahedral B crystallographic sites indicate that Fe atoms in the unit cell occupy more than eight tetrahedral sites implying much stronger A–O–B superexchange interactions. Clearly, the structural and magnetic properties of the spinel ferrites are found to be a complex function of synthetic route and the processing parameters. The novel enhanced magnetic properties of the nanoparticles can be beneficial for its potential applications.

Acknowledgements

S.V. gratefully acknowledges Department of Science and Technology (DST) India, sanction No. SR/FTP/CS-09/2007 for research grant. Research support from DST nanoscience unit of IISER, SR-NM/NS-42/2009 is also acknowledged.

References

[1] A. Goldman, Modern Ferrite Technology , Van Nostrand Reinhold, New York, 1990.
[2] M. Pardavi-Horvath, J. Magn. Magn. Mater. 215–216 (2000) 171.
[3] J. Smit, H.P.J. Wijn, Ferrites , Philips Technical Library, Eindhovan, The Netherlands, 1959, p. 158.
[4] Q.A. Pankhurst, J. Connolly, S.K. Jones, J. Dobson, J. Phys. D: Appl. Phys. 36 (2003) R167.
[5] M. Shinkai, J. Biosci. Bioeng. 94 (2002) 606.
[6] M. Zahn, J. Nanopart. Res. 3 (2001) 73.
[7] D.L. Leslie-Pelecky, R.D. Rieke, Chem. Mater. 8 (1996) 1770.
[8] R.H. Kodama, J. Magn. Magn. Mater. 200 (1999) 359.
[9] Z.X. Tang, C.M. Sorensen, K.J. Klabunde, G.C. Hadjipanayis, Phys. Rev. Lett. 67 (1991) 3602.
[10] C. Upadhyay, H.C. Verma, S. Anand, J. Appl. Phys. 95 (2004) 5746.
[11] B. Ghosh, S. Kumar, A. Poddar, C. Mazumdar, S. Banerjee, V.R. Reddy, A. Gupta, J. Appl. Phys. 108 (2010) 034307.
[12] R. Ganguly, I.K. Puri, WIREs Nanomed. Nanobiotechnol. 2 (2010) 382.
[13] J. Giri, P. Pradhan, V. Somani, H. Chelawat, S. Chhatre, R. Banerjee, D. Bahadur, J. Magn. Magn. Mater. 320 (2008) 724.
[14] S. Komarneni, E. Fregeau, E. Breval, R. Roy, J. Am. Ceram. Soc. 71 (1988) C26.
[15] A. Dias, R.L. Moreira, Mater. Lett. 39 (1999) 69.
[16] L.A. Chick, L.R. Pederson, G.D. Maupin, J.L. Bates, L.E. Thomas, G.J. Exarhos, Mater. Lett. 10 (1990) 6.
[17] S.R. Jain, K.C. Adiga, V.R.P. Verneker, Combust. Flame 40 (1981) 71.
[18] L.E. Shea, J. McKittrick, O.A. Lopez, E. Sluzky, J. Am. Ceram. Soc. 79 (1996) 3257.
[19] S. Verma, P.A. Joy, J. Appl. Phys. 98 (2005) 124312.
[20] S. Verma, H.M. Joshi, T. Jagadale, A. Chawla, R. Chandra, S.B. Ogale, J. Phys. Chem. C 112 (2008) 15106.
[21] C. Liu, A.J. Rondinone, Z.J. Zhang, Pure Appl. Chem. 72 (2000) 37.
[22] Z. Li, H. Chen, H. Bao, M. Gao, Chem. Mater. 16 (2004) 1391.
[23] J. Chatterjee, Y. Haik, C. Chen, J. Magn. Magn. Mater. 257 (2003) 113.
[24] A.J. Rondinone, C. Liu, Z.J. Zhang, J. Phys. Chem. B 105 (2001) 7967.
[25] C. Caizer, M. Stefanescu, Physica B 327 (2003) 129.
[26] N. Ponpandian, A. Narayanasamy, C.N. Chinnasamy, N. Sivakumar, J.-M. Greneche, K. Chattopadhyay, K. Shinoda, B. Jeyadevan, K. Tohji, Appl. Phys. Lett. 86 (2005) 192510.
[27] V. Sreeja, S. Vijayanand, S. Deka, P.A. Joy, Hyperfine Interact. 183 (2008) 99.
[28] S. Thakur, S.C. Katyal, A. Gupta, V.R. Reddy, S.K. Sharma, M. Knobel, M. Singh, J. Phys. Chem. C 113 (2009) 20785.
[29] P.J. Van der Zaag, A. Noordermeer, M.T. Johnson, P.F. Bongers, Phys. Rev. Lett. 68 (1992) 3112.
[30] V.A.M. Brabers, Phys. Rev. Lett. 68 (1992) 3113.
[31] P.J. Van der Zaag, V.A.M. Brabers, M.T. Johnson, A. Noordermeer, P.F. Bongers, Phys. Rev. B 51 (1995) 12009.
[32] J.P. Chen, C.M. Sorensen, K.J. Klabunde, G.C. Hadjipanayis, E. Devlin, A. Kostikas, Phys. Rev. B 54 (1996) 9288.
[33] S. Corso, P. Tailhades, I. Pasquet, A. Rousset, V. Laurent, A. Gabriel, C. Condolf, Solid State Sci. 6 (2004) 791.
[34] B.D. Cullity, Elements of X-Ray Diffraction , 2nd ed., Addison Wesley, Reading, MA, 1978, p. 99.
[35] P.C. Fannin, S.W. Charles, J.L. Dormann, J. Magn. Magn. Mater. 201 (1999) 98.
[36] L. Wang, F.S. Li, J. Magn. Magn. Mater. 223 (2001) 233.
[37] A.S. Albuquerque, J.D. Ardisson, W.A.A. Macedo, M.C.M. Valves, J. Appl. Phys. 87 (2000) 4352.
[38] B.D. Cullity, Introduction to Magnetic Materials , Addison-Wesley, Reading, MA, 1972.
[39] L.K. Leung, B.J. Evans, A.H. Morrish, Phys. Rev. B 8 (1973) 29.
[40] T.A. Dooling, D.C. Cook, J. Appl. Phys. 69 (1991) 5352.
[41] S. Morup, J. Magn. Magn. Mater. 37 (1983) 39.
[42] C.N. Chinnasamy, A. Narayanasamy, N. Ponpandian, R. Justin Joseyphus, B. Jeyadevan, K. Tohji, K. Chattopadhyay, J. Magn. Magn. Mater. 238 (2002) 281.
[43] V. Sreeja, T.S. Smitha, D. Nand, T.G. Ajithkumar, P.A. Joy, J. Phys. Chem. C 112 (2008) 14737.